A statistical analysis of the assimilative mapping of ionospheric electrodynamics auroral specification

E. A. Kihn
National Geophysical Data Center, National Oceanic and Atmospheric Administration, Boulder, Colorado, USA

A. J. Ridley
Center for Space Environment Modeling, University of Michigan, Ann Arbor, Michigan, USA

Received 23 December 2003; revised 28 January 2005; accepted 8 March 2005; published 22 July 2005.

[1] The assimilative mapping of ionospheric electrodynamics (AMIE) technique utilizes a wide range of electrodynamics measurements to determine high-latitude maps of the electric potential, electron particle precipitation (average energy and total energy flux), and ionospheric conductance (Hall and Pedersen). AMIE does this by conducting a least squares fit to the difference between the data and a background model. This fit is then added to the background model. This allows for a very stable technique with even minimal amounts of data. The background models are typically statistical models that are driven by the solar wind and interplanetary magnetic field or the hemispheric power index. This study presents results of a statistical validation of the AMIE conductance and particle precipitation calculations and quantifies how using ground magnetometer derived measurements improves upon the result obtained using only a background statistical model. Specifically, we compare AMIE using the Fuller-Rowell and Evans (1987) model of particle precipitation and ionospheric conductances to DMSP particle precipitation measurements during the period from May to November 1998. The conductances are derived from the particle precipitation using the Robinson et al. (1987) formulation. The Fuller-Rowell and Evans (1987) results show low (39–21% with increasing AE) energy flux integrals with respect to DMSP auroral passes and differences in mean electron energies. The AMIE runs, in which ground-based magnetometers were used to modify the particle precipitation using the formulation by Ahn et al. (1983) and Ahn et al. (1998), show significant improvement in correlation to the observational data. We show that it more accurately predicts the particle precipitation than when using only the background model, especially in the 1800–0300 MLT nightside sectors where solar conductance is not significant. In addition, the AMIE results show a clear increase in accuracy with increasing number of magnetometers in a sector.

Citation: Kihn, E. A., and A. J. Ridley (2005), A statistical analysis of the assimilative mapping of ionospheric electrodynamics auroral specification, *J. Geophys. Res.*, *110*, A07305, doi:10.1029/2003JA010371.

1. Introduction

[2] Understanding the complex interactions that couple the solar wind to the Earth's magnetosphere and ionosphere is an essential component of space weather prediction. Nowcasting/forecasting the high-latitude ionospheric current pattern has drawn increasing attention as a tool to support operational space weather needs. This is in part due to more models becoming available that can reliably forecast this very complex domain [*Singer et al.*, 2001].

[3] There are three primary ways of computing the high-latitude horizontal current structure. The first method is to take an electric potential pattern (produced from either an empirical relationship or a data inversion), apply ionospheric Hall and Pedersen conductance patterns to it, and calculate the horizontal current:

$$j = -\boldsymbol{\Sigma} \cdot \nabla\phi, \tag{1}$$

where j is the current, $\boldsymbol{\Sigma}$ is the conductance matrix, and ϕ is the potential. The second methodology is used extensively in global and inner magnetospheric models [*Goodman*, 1995; A. Ridley et al., Ionospheric control of the magnetospheric configuration (1): Conductance, submitted to *Annales Geophysicae*, 2005]. These models solve the divergence of the above equation for the potential and the currents:

$$j_r = \nabla_\perp \cdot (\boldsymbol{\Sigma} \cdot \nabla\phi)_\perp, \tag{2}$$

where j_r is the radial current density (provided by the magnetospheric simulation) and $\nabla_\perp$ is the divergence

0148-0227/05/2003JA010371$09.00

perpendicular to the magnetic field. Once the potential is solved for, the horizontal current can then be determined using equation (1). The MHD models infer the conductances from the field-aligned current pattern. The third methodology involves inverting magnetometer data to determine the horizontal current pattern. These current patterns can then be used to determine the electric potential given a conductance matrix.

[4] Empirical models of the ionospheric potential such as *Papitashvili et al.* [1994], *Weimer* [1996], *Ruohoniemi and Greenwald* [1996], and *Ridley et al.* [2000] can be driven solely by the upstream interplanetary magnetic field (IMF) and solar wind conditions which provide a pattern that is statistically consistent with the impending IMF condition. These models have the advantage of providing true forecasts by propagating the observed IMF condition from spacecraft such as ACE [*Stone et al.*, 1998] to the Earth [*Ridley*, 2000] arriving at a likely potential pattern. However, because they are statistically based, they cannot capture the transients in the environment that may be precisely what is needed in an operational mode. An emerging methodology using first-principles models of the magnetosphere offers promise for the future but currently is too computationally expensive to support real-time operational needs [*Ridley et al.*, 2001]. A third class of models uses various data assimilation techniques such as data inversion or spherical harmonic analysis to convert observational inputs into a global ionospheric pattern. Methods such as *Ruohoniemi and Greenwald* [1996] or KRM [*Kamide et al.*, 1981] provide a nowcast of the ionospheric potential that is consistent with current observational data and can be used to predict the short-term future evolution of the pattern. This type of model provides the current best approach to supporting near-real-time operations.

[5] It is clear that in order to determine either the potential pattern from currents (or ground-based magnetometers) or the horizontal current pattern from an electric potential pattern, it is essential to have accurate estimates of the conductance pattern. There is a secondary need for accurate specifications of the conductance: the ionospheric Joule heating is directly dependent upon the Pedersen conductivity. The Joule heating can cause the thermosphere to heat up and expand, causing significantly increased satellite drag. In addition, significant Joule heating can cause changes in temperature dependent reaction rates, thereby changing the composition of the ionosphere and thermosphere. It is therefore quite important to accurately specify the Pedersen conductance.

[6] The total conductance is divided into a solar-induced component and that resulting from precipitating particles. Models such as those presented by *Sotirelis and Newell* [2000], *Fuller-Rowell and Evans* [1987], and *Spiro et al.* [1982] describe the general patterns for electron precipitation binned by the observed space weather conditions. The solar-induced component is typically described by *Brekke et al.* [1974], *Horwitz et al.* [1978], *Vickrey et al.* [1981], *Wallis and Budzinski* [1981], *Moen and Brekke* [1993], or *Lilensten et al.* [1996]. This study is focused on quantifying how well the assimilative mapping of ionospheric electrodynamics (AMIE) technique [*Richmond and Kamide*, 1988; *Richmond*, 1992] is able to create a conductance pattern using magnetometer and hemispheric power index (HPI) data as inputs. This is the first of several studies which will quantify, statistically, the performance of the AMIE technique and its background models in terms of their accuracy in estimating the electric potential, conductance, ground magnetic perturbations, and derived parameters.

[7] AMIE is a data inversion technique that blends electrodynamic observations and statistical representations to produce estimates of high-latitude conductances, electric fields, and electric currents. The technique is designed to incorporate a large number of observed fields, thereby increasing the number of data types and sources and hence the accuracy of the specification. When operating in a real-time or near real-time mode (i.e., rtAMIE), the available data is typically quite limited. Using rtAMIE means using only the IMF data available from ACE, the HPI measured in the last few hours, the $F_{10.7}$, and the ground magnetometer data available from the various observing chains, typically $\sim$20 high-latitude stations.

[8] We have collected, cleaned, and quality controlled 5 years (1997 to 2001) of global magnetometer data and used this, as well as the available solar wind and IMF, HPI, $F_{10.7}$, and D_{st} data to produce an archive of AMIE runs at 1-min resolution [*Ridley and Kihn*, 2004]. Because of the uneven station coverage between hemispheres, for this study we have chosen to compare the northern hemisphere AMIE predictions of precipitating electron energy and flux with DMSP satellite observations for May to November 1998 (7 months). The ground station data available in this period is very stable and the typical coverage is shown in Figure 1. Approximately 65 magnetometer stations were used for the electron precipitation calculations. Approximately 90 high-latitude and midlatitude stations were used in the calculation of the electric potential pattern, although the potentials are not described here. The auroral magnetometers were also used to calculate the different auroral electrojet indices (AL, AU, and AE). In this study, when we use HPI data, we take the DMSP satellite estimate from the time closest to a given AMIE run. Thus most likely the estimate is from the particular satellite orbit being studied.

[9] We use the DMSP SSJ/4 data [*Hardy et al.*, 1984] archived at the National Geophysical Data Center (NGDC) to provide the observational comparison. This comes to over 11,000 northern polar cap crossings by the four spacecraft (F11–F14) available during this time. We do not address intersatellite differences and instead look only at the composite data binned in MLT, magnetic latitude, and activity level, as determined from the AL index found from the available auroral magnetometers.

2. Methodology

[10] AMIE is typically referred to as a least squares data inversion technique. AMIE is different than many data inversion techniques in that it subtracts a background pattern from the data and fits to the differences between the data and the background pattern. In addition, AMIE uses a covariance matrix to constrain the fit, allowing for large spatial gaps between data points without spurious maxima and minima in the fitted quantity. This technique allows AMIE to force the fit result away from the data to be close to zero, which makes it a very stable technique. This methodology is similar to a Kalman filter.

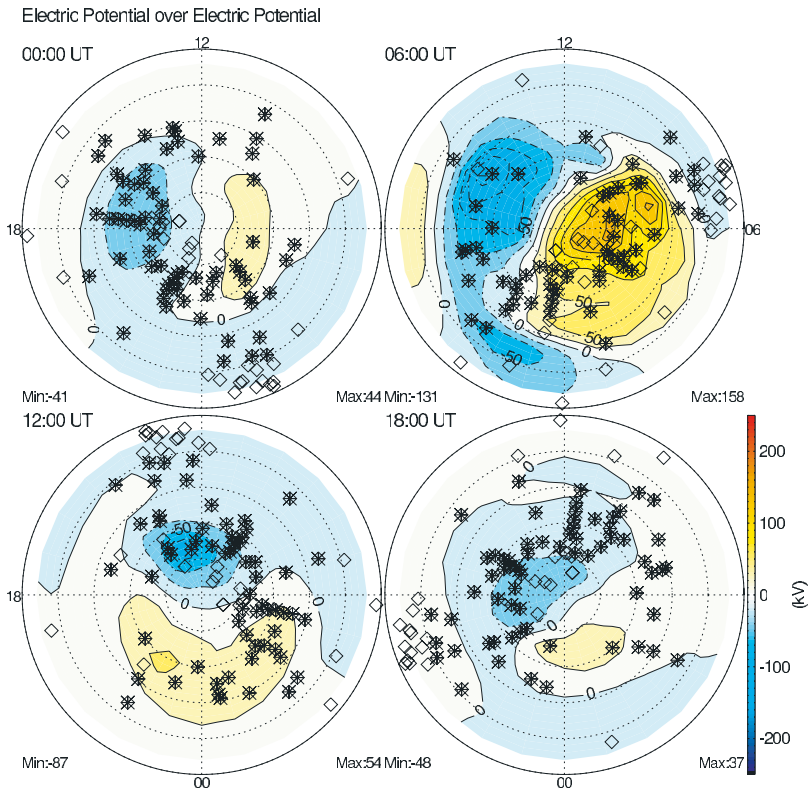

Figure 1. These plots show the ground-based magnetometer coverage for four different universal times (UTs) of 4 May 1998. Each diamond represents a magnetometer station that was used in the electric potential calculation, while the stars represent stations used to calculate the particle precipitation.

[11] AMIE can complete a total of four data inversions: (1) the average energy of precipitating electrons ($\overline{E}$); (2) the total energy flux of precipitating electrons (Φ_E); (3) the Hall (Σ_H) and Pedersen (Σ_P) conductance; and (4) the electric potential. The user must select to fit either the electron precipitation information and/or the Hall and Pedersen conductances. If the user selects the precipitation only, the Hall and Pedersen conductances are derived from the relationships formulated by [*Robinson et al.*, 1987]:

$$\Sigma_P = \frac{40\overline{E}}{16+\overline{E}^2}\Phi_E^{1/2} \tag{3}$$

and

$$\Sigma_H = 0.45\left(\overline{E}\right)^{0.85}\Sigma_P. \tag{4}$$

[12] In order to understand how well or how poorly the AMIE technique reproduces the different ionospheric electrodynamic quantities, it is best to start from the root parameter. This is the background model of the electron precipitation and the conductance pattern. AMIE takes this background pattern, subtracts it from the data, and inverts that to determine a difference pattern. This is added back to the background pattern. The Hall conductance pattern is then used in combination with the magnetometer data to determine an electric potential pattern. It is the goal of this study to examine how well this method of conductance pattern determination is working in AMIE.

[13] In our usage of AMIE for this study, the data (magnetometers, IMF, and HPI) are read in by AMIE. Estimates of the conductance are derived from the magnetometer data using *Ahn et al.* [1983, 1998] (henceforth Ahn) where applicable (shown in Figure 1 as stars) and the magnetometer data is converted to a total Hall and Pedersen conductance. The solar conductance is subtracted from the total conductance: $\Sigma_{Ha} = \sqrt{\Sigma_{Ht}^2 - \Sigma_{Hs}^2}$, where Σ_{Ha} is the Hall conductance due to auroral precipitation, Σ_{Ht} is the total Hall conductance, specified by the Ahn formulation, and Σ_{Hs} is the Hall conductance specified by the model of the solar conductance. The same is done for the Pedersen conductance. *Ridley and Kihn* [2004] gives the formulation for the solar conductance used within AMIE. Each "measurement" (derived through Ahn) of the auroral Hall and Pedersen conductance is then converted into a total energy flux and average energy using the *Robinson et al.* [1987] formulation (as described by *Ahn et al.* [1998]). These "measurements" of the precipitation are used in the inversions within AMIE, as described above. The background conductance model used in this study is described by *Fuller-Rowell and Evans* [1987] (henceforth FRE). We point out here that a limitation of Ahn is that it applies primarily to the 1800–0300 MLT sectors. This is because the average energy of the particles precipitating in the noon sector is small and their contribution to the conductance is minimal. Therefore a magnetic disturbance recorded around noon is seldom associated with significant conductance enhancement. As a result, there are not enough data points

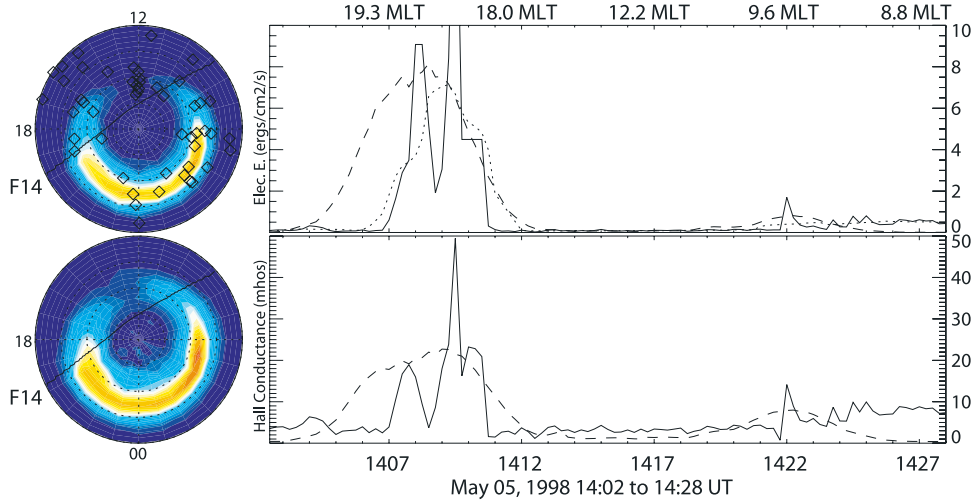

Figure 2. A comparison between total electron precipitation in mW/m and Hall conductances in mhos calculated from the assimilative mapping of ionospheric electrodynamics (AMIE) technique (dashed lines) using only ground-based magnetometer and DMSP J4 measured electron precipitation and estimated Hall conductances (solid lines) using the *Robinson et al.* [1987] formulation. The dotted line in the top plot is a 10 point running average of the DMSP measured electron precipitation. The plots on the left show the AMIE results of electron energy (top) and Hall conductance (bottom) with the locations of the ground-based magnetometers and DMSP satellite overplotted. In these plots, the magnetic pole is at the center, while the outer circle is at 50°. Dusk is to the left, while the Sun is toward the top of the figure. The start of the DMSP pass is indicated as an "F14" (i.e. the name of the satellite).

capturing conductance enhancement on the dayside to include in the Ahn model.

[14] While there are obviously many assumptions that go into using the magnetometers to determine the particle precipitation, there are advantages to this technique: (1) magnetometers offer a consistency in location of measurement that many other techniques (such as in situ satellite measurements) do not offer; (2) imagers from satellites only view the total auroral oval for a small period of time during the day, while magnetometers offer a semi-global view of the auroral oval all day, every day; (3) many of the other techniques, such as global imagery from satellites and incoherent scatter radar measurements of the conductance, have many assumptions that also enter into the calculations; (4) this technique allows a determination of the global electric potential for many years on a 1 min timescale, which cannot be done by any other technique with nearly the same global scale coverage; and (5) because there are magnetometer stations available in near-real-time and since the input to these models is solely the ground magnetic disturbance data, these models are likely candidates to be employed by real-time techniques.

[15] One part of the process that needs to be clarified is that the FRE model is presented in terms of characteristic energy and AMIE needs to convert this to an average energy to complete the inversion. To do this, AMIE assumes a Maxwellian particle spectrum and must choose the temperature that best matches either the correlation with the TIROS Hall conductance, Pedersen conductance, or the ratio of the two. In our study we choose the latter. It is possible to utilize other background models, such as by *Sotirelis and Newell* [2000] or *Hardy et al.* [1985], but it is beyond the scope of this initial investigation to compare multiple background models.

[16] Very few studies have been published on how well AMIE reproduces data sets that were not used in the inversion. *Lu et al.* [2001] investigated the sensitivity of AMIE during a single time period. No study has been published that statistically validates AMIE. *Ridley and Kihn* [2004] investigated the relationship between the Polar Cap Index and AMIE cross polar cap potential, electric field, and polar cap area for a period of 5 years (1997–2001) but did not consider the comparison a validation of either.

[17] In this study, we compare independent observational data to both the background FRE model and the AMIE results when the magnetometers have been used to modify the FRE patterns, as described above. Both model patterns are output on a magnetic local time (MLT) by magnetic latitude (APEX coordinate) grid. The resolution of the results for this period is 2° latitude by 1 hour of MLT.

[18] The DMSP electron precipitation data is taken in 30 logarithmically spaced bins between 30 eV and 30 keV 4 times per second. In our study only the spectrum above 500 eV is used. This is because much of the number flux is in the low-energy electrons but the spectrum is non-Maxwellian there [*Rich et al.*, 1987]. An average energy and total energy flux are computed for each 1/4 s, and these quantities are averaged into 15 s bins. This gives a spatial resolution of approximately 0.9° on a great circle or about 100 km.

[19] Many of the DMSP orbits contain extremely large spikes in the total energy flux. These are most likely caused by intense small-scale auroral arcs, which neither the FRE model nor AMIE can reproduce since they are significantly smaller than the grid resolution. To attempt to minimize the biasing of the small-scale auroral arcs on the statistical analysis, we weight the different parameters (i.e., energy flux, Hall conductance) by a factor based on how smooth

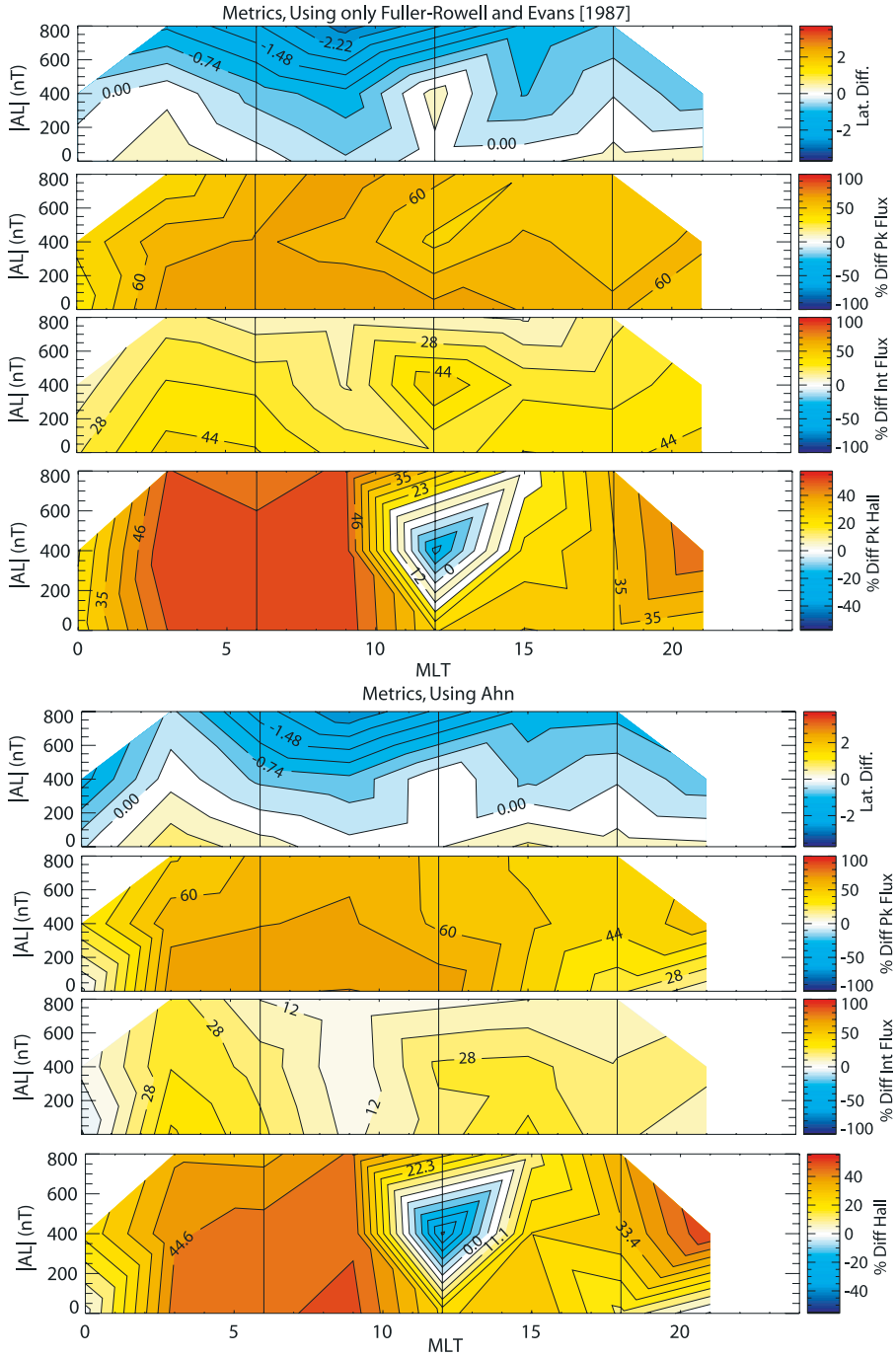

Figure 3. The top four plots are comparisons between DMSP and AMIE using the *Fuller-Rowell and Evans* [1987, hereinafter referred to as FRE] background model, while the bottom four plots are comparisons between AMIE using the magnetometer data and the DMSP data. In each group of four plots, the top plot is the latitudinal difference between the location of the measured and modeled peak auroral flux, the second plot is the percent difference between the modelled and measured peak auroral flux, the third plot is the percent difference between the measured and modelled integrated flux, and the fourth plot summarizes the difference in peak Hall conductance. The vertical axis the activity level, while the horizontal axis is the magnetic local time of the measurement.

the auroral oval is over that particular pass. This factor is the cross-correlation between the 100 km resolution DMSP data and the DMSP data smoothed over an approximately 1000 km moving window. Any large spike in the 100 km resolution data causes a decrease in the cross-correlation. The 1000 km moving window allows large-scale features, such as double ovals, to have high correlations. A graphic illustrating a typical comparison is shown in Figure 2. In each figure that shows the DMSP data, the 1000 km moving window average is shown as a dotted line in the total energy flux plot.

Table 1. Assimilative Mapping of Ionospheric Electrodynamics (AMIE) Conductance Comparisons for $|AL| < 400$ nT

MLT		0–3	3–6	6–9	9–12	12–15	15–18	18–21	21–24	Mean
%-Diff Int Flux	FR-E	24.9	48.2	45.0	33.0	26.0	44.6	43.6	47.2	39.1
	Ahn	−8.3	37.7	22.9	0.35	6.9	30.4	16.5	8.9	14.4
%-Diff Pk Flux	FR-E	31.7	72.4	74.1	73.4	65.0	65.9	60.3	51.5	61.8
	Ahn	0.47	70.1	73.0	72.1	58.4	43.4	26.9	10.7	44.4
%-Diff Pk Hall	FR-E	23.6	53.2	53.2	56.7	26.0	34.3	33.8	27.9	38.6
	Ahn	3.0	48.7	49.5	53.7	23.2	32.8	17.3	1.9	28.8
Lat. diff (Peak)	FR-E	0.37	1.3	1.1	1.0	3.2	1.2	0.86	0.9	1.2
	Ahn	0.14	1.0	0.85	0.69	3.4	1.4	0.67	1.0	1.1
Lat. diff (CC)	FR-E	−1.6	0.2	−0.03	−0.1	0.1	−1.2	−1.2	−1.1	−0.6
	Ahn	−1.3	−0.1	−0.3	−0.3	0.2	−1.0	−1.2	−1.2	−0.7
CC w/DMSP	FR-E	0.37	0.63	0.61	0.61	0.34	0.2	0.3	0.39	0.43
	Ahn	0.41	0.63	0.62	0.62	0.33	0.21	0.32	0.43	0.45
Num Samples		295	362	1948	1808	91	858	1743	109	-

[20] As each DMSP orbital path crosses the patterns, the results are linearly interpolated to the location of the satellite at the given time, and a comparison is made with the observed total electron energy flux and the Hall conductance calculated from observations from the spacecraft. We choose these two quantities because the electron energy flux is quite important in determining the electron energy deposition and ionization rates throughout the atmosphere and the Hall conductance is directly relevant to the inversion of the ground-based magnetic perturbations. It should be noted that the pattern closest in time to the DMSP measurement is used in the comparison. In order to summarize the results across multiple passes, the data are divided into dawn and dusk flight segments. Each segment is then compared with the model results in terms of percentage difference in peak electron flux value (%-Diff Pk Flux), the percentage difference integral electron flux (%-Diff Int Flux), the percentage difference in peak Hall value (%-Diff Pk Hall), and the latitude difference of the observed peak flux (Lat. diff (Peak)). This is done for both AMIE using only the FRE model and including the Ahn technique.

[21] The integral flux is defined as a line integral of the total energy flux over approximately 2000 km, centered on the location of the DMSP measured peak energy flux. This is meant to give an indication of the total energy flux within the auroral oval for that particular region. If, for example, the modeled patterns had a too small maximum peak flux and it smeared out the auroral oval too much, the total auroral energy going to the ionosphere over that region may still be correct. The DMSP and model integrals are differenced and then divided by the maximum of the two integrals to come up with a percentage difference. If the number is positive, then the DMSP energy flux is larger; if it is negative, the model energy flux is larger.

[22] We further calculate the zero lag cross-correlation with the models (CC w/DMSP), then each orbit is split into ascending and descending segments and the individual segments are shifted to where the cross-correlation is maximized. This is recorded as the (Lat. diff (CC)), which provides a measure of the models' success in size and placement of the auroral oval.

[23] The results produced above are binned relative to different criteria, such as the calculated lower auroral electrojet (AL) index, number of magnetometers in a sector, and MLT. This allows the investigation of any systematic differences due to activity level and local time. In addition, it allows a quantitative determination of how well the patterns are improved by adding magnetometers in given sectors.

3. Results

[24] The results of the study are summarized in Tables 1–4 and in Figure 3. Several points are of obvious interest in the resulting data. The first is that the flux calculated from FRE is much lower than that observed by DMSP SSJ4 at low activity levels. This is true both in the peak flux, which tends to be over 60% under the observed values, and the integral flux, which is nearly 40% too low. Both of these show improvement under more active conditions though. For example, comparing Tables 1–3, the percent difference

Table 2. AMIE Conductance Comparisons for $400 < |AL| < 1000$ nT

MLT		0–3	3–6	6–9	9–12	12–15	15–18	18–21	21–24	Mean
%-Diff Int Flux	FR-E	12.0	37.6	35.6	19.1	-	32.1	32.6	40.8	30.0
	Ahn	−0.1	28.0	22.0	0.7	-	23.4	16.7	26.2	16.7
%-Diff Pk Flux	FR-E	42.7	66.1	69.6	65.1	-	62.9	56.1	61.4	60.6
	Ahn	34.6	60.6	66.4	62.3	-	54.4	45.3	55.2	54.1
%-Diff Pk Hall	FR-E	20.4	57.7	56.2	54.7	-	31.3	34.7	51.8	43.8
	Ahn	23.3	44.2	49.5	49.6	-	34.6	33.4	55.7	41.5
Lat. diff (Peak)	FR-E	0.1	0.6	−0.0	−0.3	-	−0.2	0.3	−1.9	−0.2
	Ahn	−1.3	0.2	−0.1	−0.4	-	−0.3	0.6	−1.3	−0.2
Lat. diff (CC)	FR-E	−0.7	0.0	−0.8	−0.8	-	−1.3	−0.8	−1.6	−0.9
	Ahn	−1.3	−0.5	−0.8	−0.9	-	−1.1	−0.4	−1.5	−0.9
CC w/DMSP	FR-E	0.68	0.79	0.74	0.69	-	0.36	0.56	0.68	0.64
	Ahn	0.63	0.80	0.75	0.69	-	0.37	0.56	0.62	0.63
Num Samples		24	46	177	172	1	84	244	8	-

Table 3. AMIE Conductance Comparisons for $|AL| > 1000$ nT

MLT		0–3	3–6	6–9	9–12	12–15	15–18	18–21	21–24	Mean
%-Diff Int Flux	FR-E	-	33.9	18.0	17.7	-	9.9	27.5	-	21.4
	Ahn	-	17.7	6.7	−1.5	-	3.8	15.3	-	8.4
%-Diff Pk Flux	FR-E	-	50.1	65.1	73.9	-	51.4	51.5	-	58.4
	Ahn	-	43.0	59.2	64.3	-	47.6	45.3	-	51.2
%-Diff Pk Hall	FR-E	-	53.7	52.3	57.8	-	20.6	36.4	-	44.2
	Ahn	-	39.3	40.5	50.4	-	21.9	38.5	-	38.1
Lat. diff (Peak)	FR-E	-	−0.6	−1.5	−3.3	-	−1.8	−1.8	-	−1.8
	Ahn	-	−0.8	−1.7	−3.2	-	−1.8	−1.8	-	−1.9
Lat. diff (CC)	FR-E	-	−1.0	−2.3	−3.0	-	−0.9	−1.3	-	−1.7
	Ahn	-	−0.9	−2.1	−3.0	-	−0.9	−1.1	-	−1.6
CC w/DMSP	FR-E	-	0.77	0.69	0.60	-	0.49	0.63	-	0.64
	Ahn	-	0.79	0.70	0.59	-	0.49	0.59	-	0.63
Num. Samples		1	6	41	29	0	21	58	1	-

in the integral flux (“%-Diff Int Flux”) decreases from 39% to 21% as AL decreases from low activity (i.e., >-400 nT) to high activity (i.e., <-1000 nT). This trend is smaller in the percent difference of the peak flux (i.e., “%-Diff Pk Flux”). Interestingly, the trend reverses in the peak Hall conductance. As the activity level increases, the deviation from the data increases. This means that the difference is in the average energy calculation, since the peak Hall conductance is closely tied to the average energy, as equations (3) and (4) illustrate.

[25] A second result is that the inclusion of the magnetometer data (i.e., the AMIE results including the magnetometer data via the Ahn formulation) appears to help in the integrated and peak flux specification at all MLTs and at all activity levels. The level of improvement in the results varies dramatically from one bin to another, but there is improvement everywhere. This result is seen most significantly in the 1800–0300 MLT region where solar conductance is minimal. Interestingly, the improvement in the specification of the peak Hall conductance by including the magnetometer data is less than the improvement in the peak and integrated flux. Once again, this probably has to do with the prediction of the average energy flux.

[26] Another result from the tables is that with respect to the placement of the peak flux, both FRE and AMIE do reasonably well. The difference in peak is comparable to the grid resolution of the results. Notice, however, that as the activity level increases the values flip from positive to negative, indicating that for low activity the models place the auroral boundary too low and for high activity levels they place the boundary too high (see Figure 3), so the range of the model aurora is more restricted in going from high latitudes during low activity periods to lower latitudes in high activity periods. Interestingly, AMIE with Ahn does not show any marked improvement in the peak placement over the FRE model. This probably owes to two factors: (1) the AMIE grid resolution precludes the shift provided by including magnetometer data reflecting as actual grid cell changes, and (2) the occasional peak in the polar cap region as observed by DMSP is captured by neither the FRE model nor AMIE. Within AMIE, this is due to the lack of high-latitude stations. Also of note is the fact that the Lat. diff (CC) is always negative, indicating a better correlation when the model is shifted poleward. It is unclear the cause of this, but we suspect it has to do with all the polar precipitation observed by DMSP, especially at low activities, which is not captured by AMIE.

[27] The value of the cross-correlation coefficient (zero lag cc w/DMSP) is fairly low (0.5–0.6) in most cases, indicating that while both models are getting the gross shape of the aurora, they miss significant elements of the fine structure. The cross-correlation shows a definite improvement with increasing activity level in both models, probably because as the activity increases the auroral boundary takes a more definite shape.

[28] Table 4 shows how the number of magnetometers in a given sector influences the AMIE solution. This table shows that there is marked improvement in the peak and integral flux estimate when there are multiple magnetometers in a sector. The result shows positive influence on the estimate starting with one or two up through five magnetometers in a sector. There is a significant jump in performance between zero (i.e., the FRE model with no data included) and five magnetometers. The eventual errors of $\sim$30% are within the error range given in the Ahn formulation [*Ahn et al.*, 1998]. It is interesting to note that in nearly all cases the AMIE total energy flux and peak Hall conductance values are below the observations. Another result is that percentage difference in the peak flux and peak Hall conductance underestimates increase with increasing activity level. This means that AMIE is underpredicting the peak flux and peak Hall conductances more as the activity level increases. This does not seem to be true for the integral flux, however, indicating that the model is getting the total flux of particles into the auroral oval correct but not in a

Table 4. A Comparison Between AMIE Results With a *Fuller-Rowell and Evans* [1987] Background and a Modified *Ahn et al.* [1983, 1998] Magnetometer Driven Conductance and the DMSP Measurements as a Function of the Number of Magnetometer Stations Above 50° in a MLT Sector Through Which the Orbit Passes

Num. Magnetometers	AL	0	1–2	3–4	5+
% Diff Int Flux	Low	31.8	19.1	12.0	10.9
	Mid	47.4	17.5	13.7	15.4
	High	-	23.4	18.1	12.5
% Diff Pk Flux	Low	46.3	38.1	21.6	18.7
	Mid	69.1	52.0	45.0	40.6
	High	-	65.7	48.8	38.5
% Diff Pk Hall	Low	27.2	17.5	11.9	9.9
	Mid	46.0	30.7	30.4	31.3
	High	-	49.1	44.8	35.6
Num. Samples	Low	55	298	250	1523
	Mid	14	46	41	172
	High	3	14	8	35

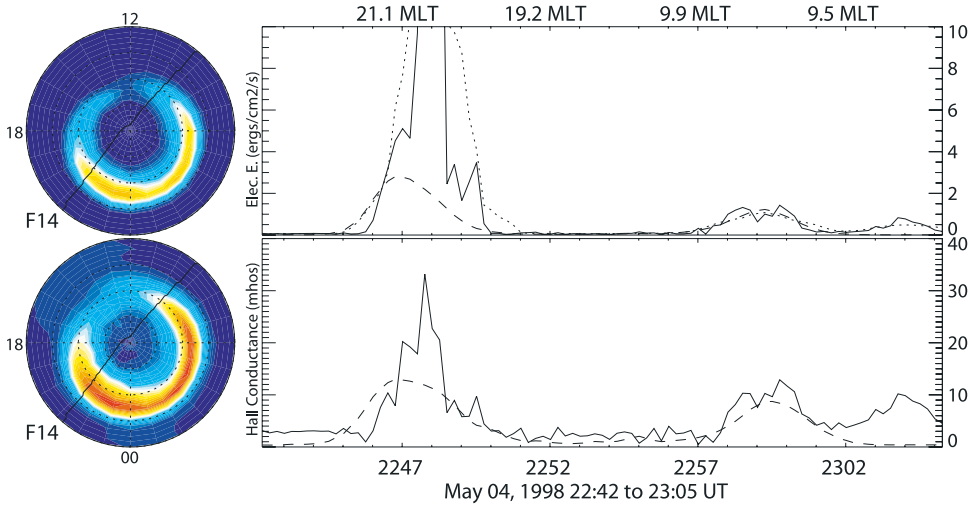

Figure 4. These plots show a comparison of the DMSP J4 measurements and the FRE patterns for 4 May 1998 in the same format as Figure 2.

sharp enough region. In the discussion section below we present possible explanations for some of the model deficiencies compared with observational data.

4. Discussion

[29] AMIE can use a wide variety of data to complete its inversions. These include incoherent scatter radar line of sight measurements and conductance estimates, high-frequency radar line of sight data (such as from SuperDARN), in situ measurements of flow velocities, particle precipitation, and magnetic fields (such as from the DMSP, NOAA, UARS, FAST, and other satellites), imaging data of the aurora (such as from POLAR UVI or IMAGE FUV), and ground-based magnetic field measurements. However, the most readily available data on this list are the ground-based magnetic field measurements. AMIE is therefore most often run including a significant amount of magnetometer data.

[30] Some advantages with using ground-based magnetometer data are (1) consistency of data during an event, (2) global data coverage, (3) data availability, and (4) relative ease of use in statistical studies. Ground-based magnetometer data also have some disadvantages: (1) lack of coverage over the oceans; (2) magnetometers are integrating devices, so they tend to smear out small-scale features; and, probably the most significant, (3) the ionospheric Hall conductance must be accurately specified in order to determine the true ionospheric electric field above a ground-based magnetic field measurement.

[31] Because there are both advantages and disadvantages with these measurements, AMIE is usually run with other data sets, which may complement the magnetometer data. For example, SuperDARN radars measure the ion flow velocities in the *F* region of the ionosphere. Since this is a (more) direct measurement of the electric field, it complements the magnetometer's need to use the conductance. Conversely, SuperDARN radar measurements drop out in large portions of the high-latitude region during some events. The magnetometer data offer a temporal consistency which allows studies of how the ionospheric convection

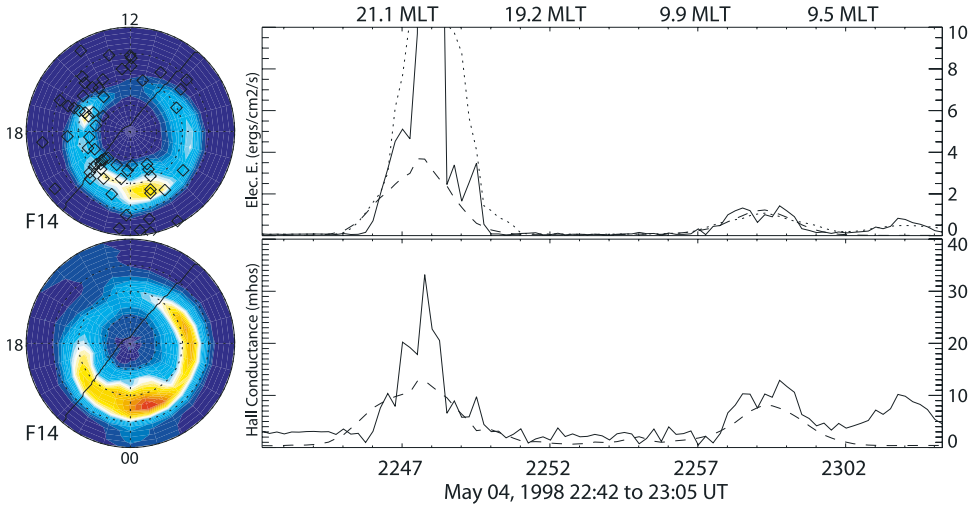

Figure 5. A comparison of the AMIE derived electron precipitation and Hall conductance with the DMSP J4 measurements on 4 May 1998.

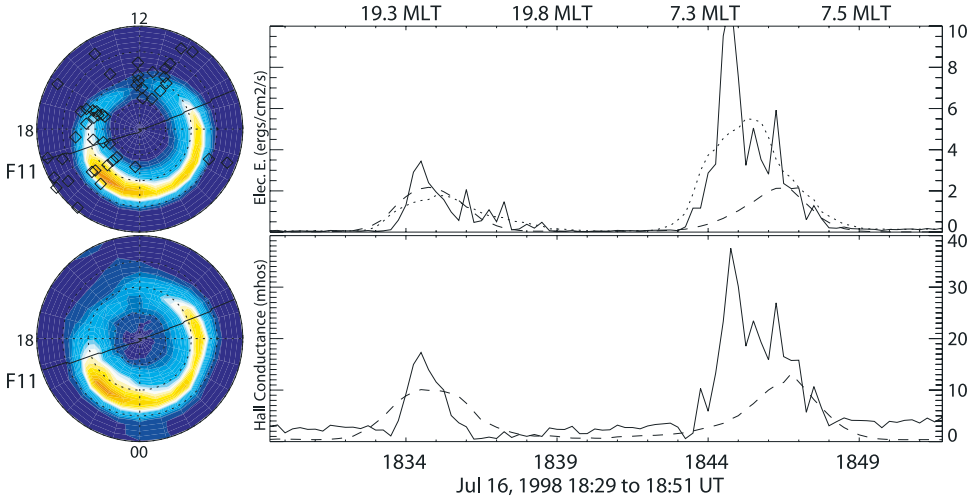

Figure 6. An example of a pass in which the ascending part of the pass had very good station coverage while the descending part of the pass had poor coverage.

(and auroral activity) may change with time on a global scale. For example, the study by *Ridley et al.* [1998] presents global patterns of the changing convection using magnetometer data, while *Ruohoniemi and Greenwald* [1998] shows how the convection may change at two locations directly using SuperDARN data. Given all these possible configurations, it is important to emphasize that our study focuses on AMIE run using only magnetometer data.

[32] Looking first at the *Fuller-Rowell and Evans* [1987] model based runs as presented in Tables 1–3, several points become apparent. The first is that this model underestimates the electron energy flux. It is true for both peak flux and integral flux. Since this is a statistical model and therefore likely to flatten sharp peaks, the result with respect to peak flux is somewhat expected. However, even the integrated flux is low by approximately 40%. There are several possibilities that could explain the discrepancy. The FRE model uses as input the hemispherical power index (HPI), which unfortunately varies rather slowly as compared with the cross-polar flight of DMSP. This means that while DMSP is sampling the instant particle measurement, the FRE pattern is fixed to some moment along the flight. If it were possible to generate a higher-cadence HPI, this might show some improvement. Another possible cause for a significant error is the difference between the NOAA-TIROS instrument package (which was used to build the FRE model) and the DMSP-SSJ4 instrument, which was used in the comparisons and also used to estimate the HPI needed to run the FRE model.

[33] Preliminary work comparing the two systems over a long term with respect to HPI measurements indicates that a 20–40% difference between instruments is not unlikely (B. Emery, private communication, 2005). Figure 4 shows a typical result using the FRE model. The peak value, while approximately in the correct location, is well under the observation and the total integral flux (i.e., the area under the curve) is also much too small.

[34] A good example of the improvement gained by including the magnetometer data is shown in Figure 5. In this case the station placement is just right to get the top and the bottom of the auroral oval. Thus the model puts the flux

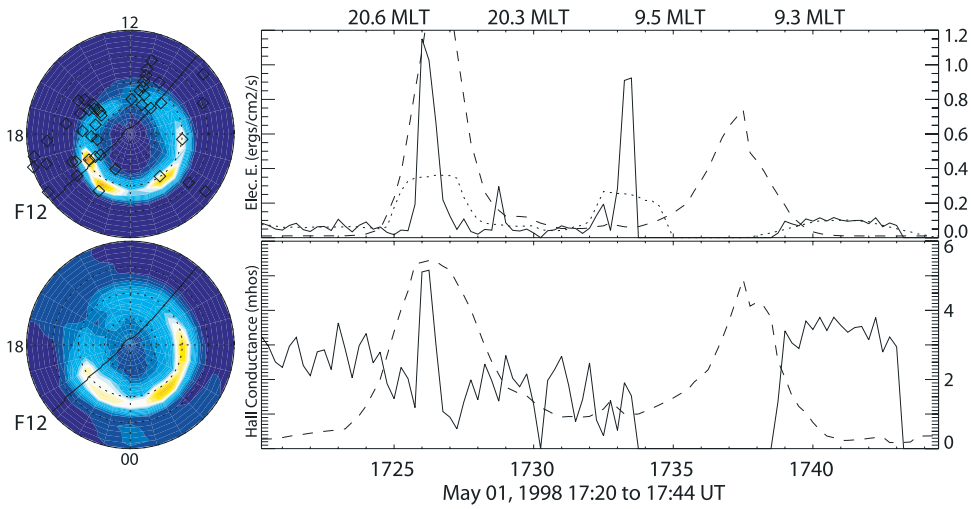

Figure 7. An example of the complex auroral structures measured by DMSP J4 on 1 May 1998.

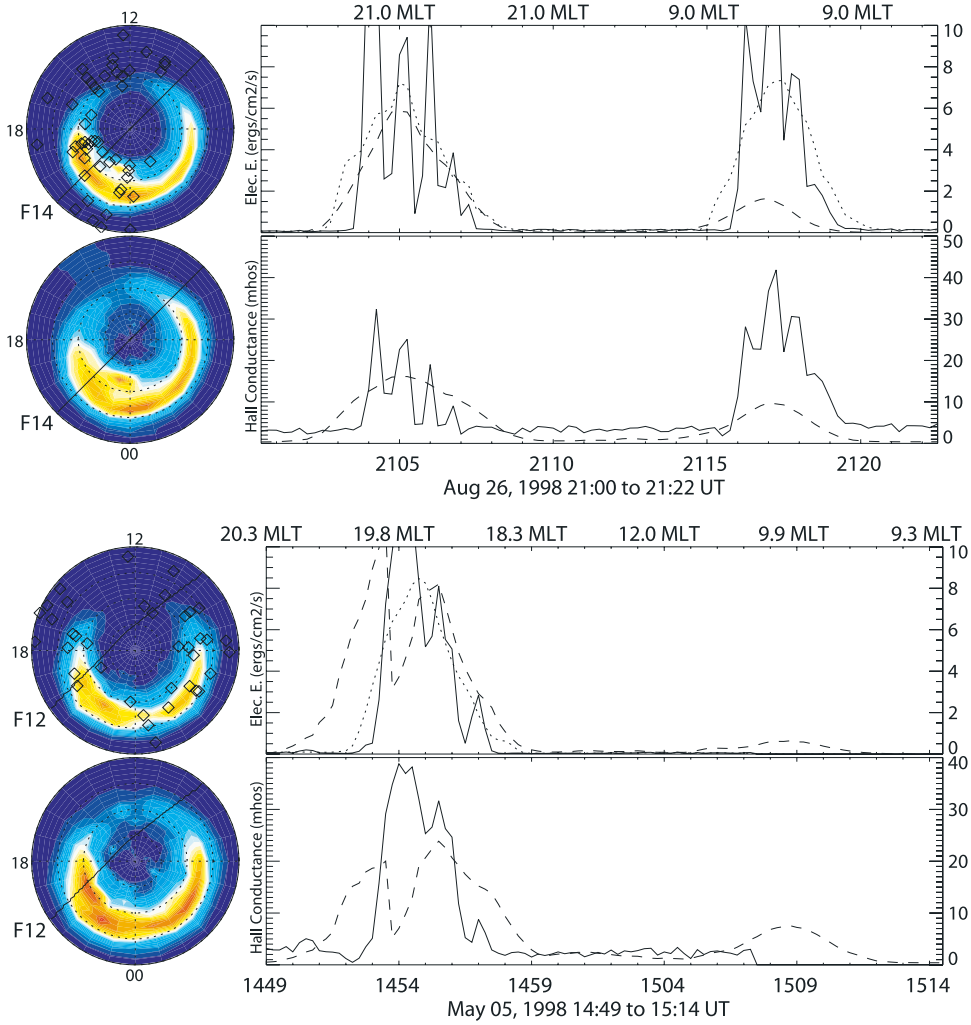

Figure 8. Two examples of highly structured aurora ovals. In the top example, AMIE smoothes out the oval too much to capture the structure. In the bottom example, AMIE produces a double oval, similar to that measured by the DMSP satellite.

in just the right place and improves the magnitude estimate. In Figure 6, we see an example where there are no stations covering the descending part of the orbit and the conductance model reverts to the FRE background estimate. In this case there are significant differences both in the electron flux and the conductance.

[35] Another problem typical in this study is the observation of auroral arcs poleward of the main aurora. Figure 7 shows an example in which AMIE seems to have the duskside main auroral oval placement correct but on the dawnside there is a big peak at higher latitude. With no stations at high latitude to correct from the background, this leads to an underestimate of peak flux and a latitude difference in the peak locations. This is observed fairly regularly on both ascending and descending segments, leading to some bias of the statistics.

[36] Figure 8 shows another problem in both models, which is dealing with highly structured auroral precipitation. As can be seen in both the Hall and electron energy flux plots, the AMIE result captures the overall shape but misses significant changes in the curve. This is despite having adequate ground coverage on the ascending segment of the pass. AMIE is capable of producing some structure even at its coarse resolution as in Figure 8, but even then it is insufficient for capturing the changes adequately.

5. Conclusion

[37] Both the *Fuller-Rowell and Evans* [1987] and AMIE technique do a reasonable job of placing the auroral oval and reproducing the magnitude of the peak flux and integrated flux. There is a strong bias toward underestimating the electron flux and Hall conductance, which is very pronounced in the FRE model. Inclusion of magnetometer data into AMIE improves this underestimation. In particular, those MLTs where *Ahn et al.* [1998] applies (1500–0300 MLT) see gains if they have any station coverage and significant improvement where there is more complete station coverage (e.g., five or more magnetometers). It provides improvement in peak e-flux, peak Hall conductance, latitude difference of the peak flux and Max-CC latitude difference. This is particularly true in the afternoon to postmidnight sectors where substantial performance gains are evident. However, even with the magnetometer data, AMIE has significant underestimates of the e-flux in the 0300–1500 MLT sector. This is because the *Ahn et al.* [1998]

formulation does not apply in this sector, so the *Ahn et al.* [1983] formulation must be used instead. Unfortunately, for use with real-time applications AMIE sees its most significant gains with five or more stations in a sector, which is seldom the case anywhere in near-real-time. The fact that AMIE relies heavily on the background model in areas in which there is little data and that the FRE model underestimates the electron energy flux with respect to DMSP is reason to investigate whether a different model, such as *Sotirelis and Newell* [2000] might produce better correlation.

[38] The study shows that AMIE is limited in its ability to reproduce fine-scale features. Even with multiple magnetometers in a sector, the result is not well correlated with the observed pattern. This is partly because of the reliance of rtAMIE on a background model and partly due to the distribution of the stations within a sector. We suggest that it would be beneficial to modify AMIE to have a variable higher-resolution grid structure across the auroral zone.

[39] A typical DMSP pass shows a great deal of structure in the polar region and these changes should be reflected in the AMIE result. It is not clear if there are any models available at this time that can produce this result using real-time inputs only.

[40] Finally, it is worth noting that in this study we specifically excluded any DMSP instruments and other satellite data from the input data (except to drive the background model, in the form of the HPI). As a data ingest model, AMIE is fully capable of ingesting the DMSP observations, and if it were possible to obtain the full data in real-time, rtAMIE could include them to produce much improved results. The NOAA HPI is available in near-real-time, so this can be (and is) used in rtAMIE to drive the background model.

[41] **Acknowledgments.** Research at the University of Michigan was supported by NSF grant ATM-9802149. The following data was used in AMIE: CANOPUS (Canadian Space Agency), IMAGE (Finnish Meteorological Institute), Measure (University of California Los Angles), Greenland coastal chains (Danish Meteorological Institute), MAGIC (University of Michigan), MACCS (Augsburg and Boston University), 210 magnetic meridian (Kyushu University and Nagoya University), and Intermagnet. Special thanks is given to Y. Kamide of STEL for his help in preparation of this manuscript.

[42] Arthur Richmond thanks Barbara Emery and J. Ruohoniemi for their assistance in evaluating this paper.

References

Ahn, B.-H., R. Robinson, Y. Kamide, and S.-I. Akasofu (1983), Electric conductivities, electric fields and auroral particle energy injection rate in the auroral ionosphere and their empirical relations to horizontal magnetic disturbances, *Planet. Space Sci.*, *31*, 641.

Ahn, B.-H., A. Richmond, Y. Kamide, H. Kroehl, B. Emery, O. de la Beaujardiére, and S.-I. Akasofu (1998), An ionospheric conductance model based on ground magnetic disturbance data, *J. Geophys. Res.*, *103*, 14,769.

Brekke, A., J. Doupnik, and P. Banks (1974), Incoherent scatter measurements of *E* region conductivities and currents in the auroral zone, *J. Geophys. Res.*, *79*, 3773.

Fuller-Rowell, T., and D. Evans (1987), Height-integrated Pedersen and Hall conductivity patterns inferred from TIROS–NOAA satellite data, *J. Geophys. Res.*, *92*, 7606.

Goodman, M. L. (1995), A three-dimensional, iterative mapping procedure for the implementation of an ionosphere-magnetosphere anisotropic Ohm's law boundary condition in global magnetohydrodynamic simulations, *Ann. Geophys.*, *13*, 843.

Hardy, D., H. Yeh, L. Schmitt, T. Schumaker, M. Gussenhoven, A. Huber, F. Marshall, and J. Pantazis (1984), Precipitating electron and ion detectors (SSJ/4) for Block SD/Flights 6–10 DMSP satellites: Calibration and data presentation, *Environ. Res. Pap.*, *902*.

Hardy, D., M. Gussenhoven, and E. Holeman (1985), A statistical model of auroral electron precipitation, *J. Geophys. Res.*, *90*, 4229.

Horwitz, J., J. Doupnik, and P. Banks (1978), Chatanika radar observations of the latitudinal distributions of auroral zone electric fields, conductivities, and currents, *J. Geophys. Res.*, *83*, 1463.

Kamide, Y., A. Richmond, and S. Matsushita (1981), Estimation of ionospheric electric fields, ionospheric currents, and field-aligned currents from ground magnetic records, *J. Geophys. Res.*, *86*, 801.

Lilensten, J., P. Blelly, W. Kofman, and D. Alcaydé (1996), Auroral ionospheric conductivities: a comparison between experiment and modeling, and theoretical $f_{10.7}$-dependent model for EISCAT and ESR, *Ann. Geophysicae*, *14*, 1297.

Lu, G., A. Richmond, J. Ruohoniemi, R. Greenwald, M. Hairston, F. Rich, and D. Evans (2001), An investigation of the influence of data and model inputs on assimilative mapping of ionospheric electrodynamics, *J. Geophys. Res.*, *106*, 417.

Moen, J., and A. Brekke (1993), The solar flux influence os quiet-time conductances in the auroral ionosphere, *Geophys. Res. Lett.*, *20*, 971.

Papitashvili, V., B. Belov, D. Faermark, Y. Feldstein, S. Golyshev, L. Gromova, and A. Levitin (1994), Electric potential patterns in the northern and southern polar regions parameterized by the interplanetary magnatic field, *J. Geophys. Res.*, *99*, 13,251.

Rich, F., M. Gussenhoven, and M. Greenspan (1987), Using simultaneous particle and field observations on a low altitude satellite to estimate joule heat energy flow into the high latitude ionosphere, *Ann. Geophys.*, *5*, 527.

Richmond, A. (1992), Assimilative mapping of ionospheric electrodynamics, *Adv. Space Res.*, *12*, 59.

Richmond, A., and Y. Kamide (1988), Mapping electrodynamic features of the high-latitude ionosphere from localized observations: Technique, *J. Geophys. Res.*, *93*, 5741.

Ridley, A. (2000), Estimation of the uncertainty in timing the relationship between magnetospheric and solar wind processes, *J. Atmos. Sol. Terr. Phys.*, *62*, 757.

Ridley, A., and E. Kihn (2004), Polar cap index comparisons with amie cross polar cap potential, electric field, and polar cap area, *Geophys. Res. Lett.*, *31*, L07801, doi:10.1029/2003GL019113.

Ridley, A., C. Clauer, G. Lu, and V. Papitashvili (1998), A statistical study of the ionospheric convection response to changing interplanetary magnetic field conditions using the assimilative mapping of ionospheric electrodynamics technique, *J. Geophys. Res.*, *103*, 4023.

Ridley, A., G. Crowley, and C. Freitas (2000), A statistical model of the ionospheric electric potential, *Geophys. Res. Lett.*, *27*, 3675.

Ridley, A., D. D. Zeeuw, T. Gombosi, and K. Powell (2001), Using steady-state mhd results to predict the global state of the magnetosphere-ionosphere system, *J. Geophys. Res.*, *106*, 30,067.

Robinson, R., R. Vondrak, K. Miller, T. Dabbs, and D. Hardy (1987), On calculating ionospheric conductances from the flux and energy of precipitating electrons, *J. Geophys. Res.*, *92*, 2565.

Ruohoniemi, J., and R. Greenwald (1996), Statistical patterns of the high-latitude convection obtained from Goose Bay HF radar observations, *J. Geophys. Res.*, *101*, 21,743.

Ruohoniemi, J., and R. Greenwald (1998), The response of high latitude convection to a sudden southward IMF turning, *Geophys. Res. Lett.*, *25*, 2913.

Singer, H., G. Heckman, and J. Hirman (2001), *Space Weather Forecasting: A Grand Challenge*, *Geophys. Monogr. Ser.*, vol. 125, pp. 23–30, AGU, Washington, D. C.

Sotirelis, T., and P. Newell (2000), Boundary-oriented electron precipitation model, *J. Geophys. Res.*, *105*, 18,655.

Spiro, R., P. Reiff, and J. L. J. Maher (1982), Precipitating electron energy flux and auroral zone conductances: An empirical model, *J. Geophys. Res.*, *87*, 8215.

Stone, E., A. Frandsen, R. Mewaldt, E. Christian, D. Margolies, J. Ormes, and F. Snow (1998), The advanced composition explorer, *Space Sci. Rev.*, *86*, 1.

Vickrey, J., R. Vondrak, and S. Matthews (1981), The diurnal and latitudinal variation of auroral zone ionospheric conductivity, *J. Geophys. Res.*, *86*, 67.

Wallis, D. D., and E. E. Budzinski (1981), Empirical models of height-integrated conductivities, *J. Geophys. Res.*, *86*, 125.

Weimer, D. (1996), A flexible, IMF dependent model of high-latitude electric potential having "space weather" applications, *Geophys. Res. Lett.*, *23*, 2549.

E. A. Kihn, National Geophysical Data Center, NOAA, Boulder, CO 80305, USA. (eric.a.kihn@noaa.gov)

A. J. Ridley, Center for Space Environment Modeling, University of Michigan, Ann Arbor, MI 48109-2143, USA. (ridley@umich.edu)